



## Discrete element modelling of normal compression of clay

John P. de Bono<sup>\*</sup>, Glenn R. McDowell

Nottingham Centre for Geomechanics, University of Nottingham, Nottingham NG7 2RD, United Kingdom

### ABSTRACT

The discrete element method (DEM) has only rarely been used to simulate clay, due to difficulties in modelling clay particle shape and capturing the various particle interactions. This paper presents a new approach to simulate clay in three dimensions using DEM, featuring realistic particle shape and a new straightforward interaction law, which is able to reproduce all well-known characteristic platelet interactions. By varying the interactions between the platelets (including both the ‘edges’ and ‘faces’), it is possible to account for a range of environmental conditions. Simple sedimentation and one-dimensional compression tests are presented, which correctly reproduce the expected behaviour, confirming the validity of the model. Particle-scale analysis reveals the influence of the platelet interactions on the bulk behaviour, and it is also shown that platelet aggregation appears to lead to a fractal distribution of aggregated ‘stack’ sizes as a means of space filling.

### 1. Introduction

This paper presents a new approach to effectively simulate a clay using the discrete element method. The discrete element method (DEM) is known as a useful numerical tool for modelling and investigating the microscopic particle-scale behaviour of granular materials (and has been used to explain several well-known phenomena observed in coarse materials such as sands). However, attempts to model clay using DEM have been few and far between, despite the microscale behaviour of clays being much less well understood compared to sands. Due to the very small clay particle size (typically smaller than  $1 \mu\text{m}$  across the longest axis), the interactions between clay particles are controlled by chemical/electrical rather than purely mechanical forces. This small particle size means that clay particle behaviour is difficult to observe *in-situ* as a clay deforms, and therefore the underlying microscale mechanisms which control the bulk behaviour of clay soil remain uncertain.

The lack of discrete, particle-scale simulations of clay is due to several issues that clay particles present. Firstly, clay particles possess shapes which are inefficient to model (such as plates or rods), as opposed to bulky and approximately spherical sand grains. Secondly, they have complex interactions requiring specialized interaction laws (most DEM simulations have typically been concerned with mechanical interactions between spherical particles). There have nonetheless been some noteworthy attempts to simulate the behaviour of clay using discrete, particle-based models: Anandarajah (2000), Yao and Anandarajah (2003), Ebrahimi et al. (2016, 2014), Sjoblom (2015) and Pagano et al. (2020) being examples. Each of these studies used a different approach to modelling both the clay particle shape and clay particle interactions. Most of the above works developed specific particle interaction laws based on either assumed microscopic parameters and environmental conditions, or were adjusted to fit known macroscopic behaviour. In this work, a general and versatile approach to modelling particle interactions is developed, which can easily capture the various known types of interaction between clay particles. The aim of the work presented here is to provide a starting point for achieving accurate DEM simulations of clay, which ultimately should lead to uncovering new insights to clay particle behaviour.

The numerical model will be introduced in Section 2, which provides a justification of the chosen modelling approach, highlighting the novel aspects. A collection of simulations is presented and analysed in Section 3. These simulations demonstrate the ability of the

<sup>\*</sup> Corresponding author.

E-mail address: [john.debono@nottingham.ac.uk](mailto:john.debono@nottingham.ac.uk) (J.P. de Bono).

model to reproduce the salient features of normal compression of clay, and also provide some tentative new insights in to the aggregation of platelets. This is followed by concluding remarks in Section 4.

## 2. Numerical model

### 2.1. Platelets

This work focuses on modelling kaolin clay—i.e. kaolinite particles, which are flat platelets and approximately hexagonal. Kaolin is one of the most commonly studied clays, is readily available for laboratory testing, and a large body of literature exists on it. Kaolin is also the clay chosen in the majority of previous numerical studies. Broadly speaking, there are two methods of modelling non-spherical particles: using rigid groups of spheres, or using convex non-spherical shapes natively. In this work, kaolinite platelets are modelled using a rigid array of spheres, as shown in Fig. 1(a), which rotates and translates as a single entity. This is the same approach used by Sjoblom (2015), Aminpour and Sjoblom (2019), in 2D by Pagano et al. (2020), and by those in the chemistry or colloidal sciences (e.g. Thuresson et al., 2013.); however both the platelets and contact model used here offer several improvements. This method of capturing particle shape was chosen due to the ease and efficiency of capturing anisotropic interactions between the platelets. Some researchers have occasionally chosen to model clay platelets using non-spherical elements such as blocks (Yao and Anandarajah, 2003), disks (Ebrahimi et al., 2016), ellipsoids (Bandera et al., 2021) or rods in 2D (Bayesteh and Hoseini, 2021). Although visually appealing, using non-spherical shapes natively means only a single contact (or interaction) may exist between any two (convex) particles, which presents several disadvantages. Firstly, it is difficult to implement a single interaction law which can take into account the relative positions and orientations of two interacting platelets. Secondly, it does not permit categorically different interactions to be defined between different parts of the platelets (e.g., between edges and faces etc.). Thirdly, contact detection algorithms for non-spherical particles are more computationally demanding compared to spheres, which means any reduction in the number of discrete elements and contacts (interactions) does not scale directly with improvements in computational time.

Using rigid arrays of spheres to model platelets means that individual interactions may exist and act between any/all possible pairs of spheres in two different platelets. This means the overall net interaction between two platelets is the cumulative sum of all

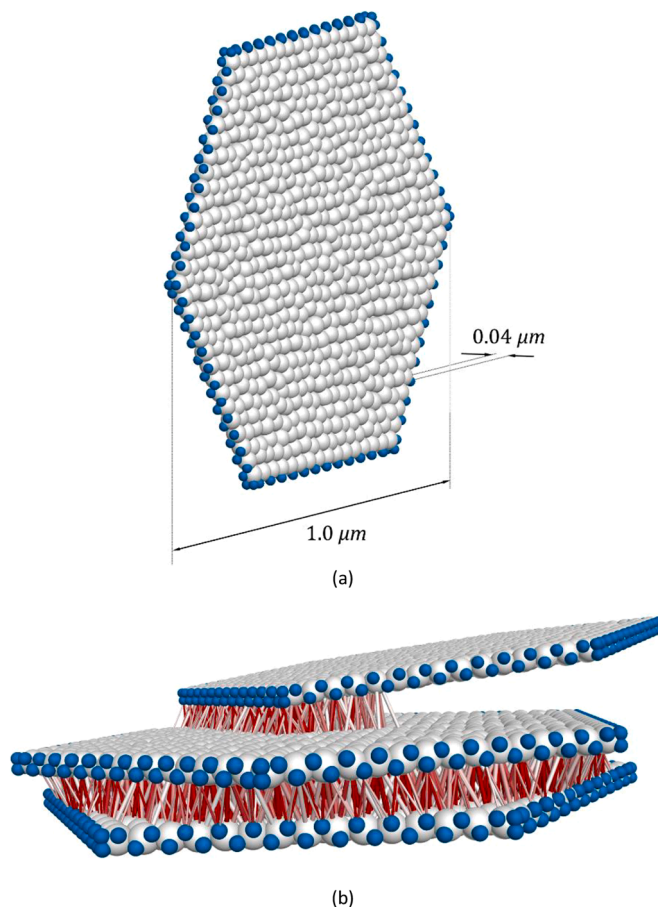


Fig. 1. Modelled kaolinite platelet made of spheres (a); expanded image showing multiple sphere-to-sphere interactions between platelets (b).

interactions between the constituent spheres, which automatically takes into account the relative positions and orientation of the two interacting platelets, illustrated in Fig. 1(b). Real kaolinite platelets have smooth surfaces; and as such, in terms of volume (and also for visualisation), the DEM platelets may be considered as rigid polyhedrons (with point charges distributed across the surfaces).

The platelets modelled in this study (Fig. 1) have a maximum diameter (corner-to-corner) of  $1\ \mu\text{m}$ , and thickness of  $0.04\ \mu\text{m}$ , giving an aspect ratio of 25, which is higher and more realistic than the previous studies using similar platelets. Real kaolinite particles vary in diameter from  $0.1$  to  $4.0\ \mu\text{m}$  (Mitchell and Soga, 2005), with aspect ratios varying between 5 and 100. The modelled particles are attributed a density of  $3.25\ \text{g/cm}^3$ , which gives a notional density of  $2.6\ \text{g/cm}^3$  ignoring the surface voids between spheres. Gravitational acceleration is set at  $10\ \text{m/s}^2$ .

Each platelet in this study contains a total of 812 spheres, 152 of which are smaller ‘edge spheres’ (blue in Fig. 1). The use of two distinct classes of spheres (*face* and *edge*) allows different interactions to be implemented between: edge-edge, edge-face, and face-face pairs of spheres (similar to Sjoblom, 2015). The edge spheres are smaller and are positioned such that for the case of two face-to-face parallel platelets, the edge spheres do not contribute significantly to the overall platelet interaction. They are also placed in a staggered ‘zig zag’ manner along each edge to provide some rotational resistance for edge-to-face interactions.

Once created, all ‘face’ spheres which are not on the perimeter, are given a small random translational displacement within the plane of the platelet (visible in Fig. 1). This removes the regular, lattice spacing, and is essential to ensure repeatable and identical interactions between platelets and prevent any interlocking effects. The importance of removing the lattice (notably absent from the earlier studies) is highlighted in de Bono and McDowell (2022).

## 2.2. Particle interactions

### 2.2.1. Background

A well-known phenomenon for colloidal particles is that two particles of a given material (such as kaolinite) often demonstrate attraction, despite possessing identical surface charges. Ordinarily, repulsive forces arise between two identical clay particles due to interacting diffuse layers of counter-ions, and any observed attraction has often been attributed to van der Waals forces, which in certain conditions were assumed to dominate over the repulsive forces. More recently however the attraction observed between like-charged platelets has been attributed to ‘ion-ion correlation’, whereby the ordering and repositioning of the (oppositely charged) counter-ions between two particles give rise to an overall attraction between the two particles at certain separations (e.g. Kjellander 1996). In any case, it is known that colloidal particles of the same charge can demonstrate both attraction and repulsion, and that increasing the electrolyte (salt) content or valence of the counterions suppresses repulsion and increases the apparent attraction. Additionally, for plate-like particles such as kaolinite, the edges are reported to possess charges independent of the faces, and may be of opposite sign, depending on the pH (Mitchell and Soga, 2005; van Olphen, 1963).

Hence the net interaction between any two clay particles depends on both the material (i.e., the clay mineral) and the environmental conditions. The various combinations possible of attractive and repulsive forces between both the edges and faces of platelets therefore leads to a range of different particle associations (‘fabrics’). Following the terminology of van Olphen (1963), in this work *flocculation* refers to general ‘edge-to-face’ and ‘edge-to-edge’ particle association, and *aggregation* refers to the ‘face-to-face’ association of platelets (shown in Fig. 2).

For two identically-charged, parallel platelets, the net interaction potential is a combination of both attractive and repulsive components, and following van Olphen (1963) can be characterised as shown in Fig. 3. The key feature in Fig. 3 is the local maximum (or lack thereof) at long-range. This long-range peak means that repulsion dominates as two particles approach from distance, which decreases the rate of particle flocculation/aggregation. Increasing the salt content (or valence of the counterions) reduces this long-range peak. Without a significant repulsive peak, attraction dominates as particles approach each other, due to the minimum in Fig. 3 at medium separation. For clarity, this region of attraction will be referred to as ‘medium-range attraction’ herein.

The edges of kaolinite particles are assumed to possess charges independent of the faces, which are overtly influenced by the pH of the pore fluid and can be either negative or positive (Mitchell and Soga, 2005; van Olphen, 1963). For oppositely-charged surfaces, simple electrostatic attraction can be assumed with no long-range repulsion, though this attraction too may be slightly reduced by the presence of an electrolyte (Melton and Rand, 1977a). At very close range, all particle interactions are repulsive.

Of the previous particle-based studies, some used a DEM-style approach to model interactions, whilst others used a Molecular

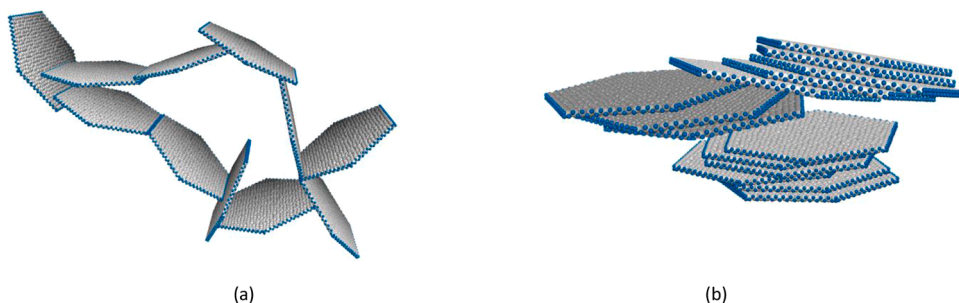


Fig. 2. Flocculated (a) and aggregated (b) platelets.

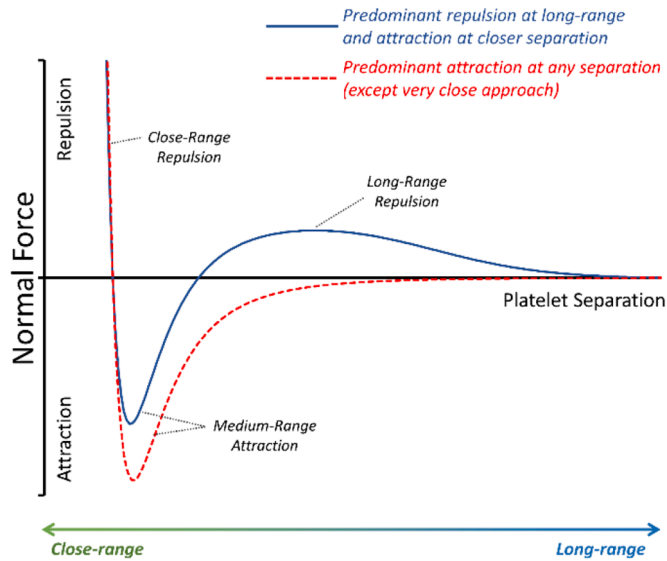


Fig. 3. Interaction for two parallel platelets as a function of separation distance

Dynamics (MD) approach. The two modelling techniques (DEM, MD) are very similar—both are concerned with computing the motion of a large number of interacting particles. Traditionally, DEM simulations are concerned with mechanical interactions between particles, with more emphasis on geometry and rotations; whereas MD simulations are traditionally focussed on (non-mechanical) long-range interactions between atoms. As such, in DEM, the particle interactions are usually defined as force-displacement laws, which compute (normal and tangential) contact forces between particles which are in a well-defined state of ‘contact’ (e.g. overlapping). In MD, the particle interactions are usually defined in terms of energy potentials, which act at long-range, and are used to deduce the forces acting upon the particles. However, it is possible to implement any potential energy function or force-displacement law as the user sees fit (e.g. force-displacement laws derived from potential energy functions which act at long-range). In this work, as in those previous studies using DEM, the interactions are modelled using ‘interaction laws’ that compute a normal force based on the separation between (non-touching) particles.

Regardless of the approach to defining interactions, for ease of implementation, some previous studies used simplified interactions, not capturing all features shown in Fig. 3 (Bandera et al., 2021; Pagano et al., 2020). On the other hand, in order to obtain platelet interactions of the correct form illustrated in Fig. 3, Yao and Anandarajah (2003), Sjoblom (2015) and Aminpour and Sjoblom (2019) calculated the interaction between two platelets as the sum of three types of forces: the diffuse layer repulsion, van der Waals attraction, and close-range repulsion. Notably, their calculations of these separate forces (such as the diffuse layer repulsion) were related to specific properties of both the clay particles and fluid. These calculations were largely based on the classic DLVO (Derjaguin-Landau-Verwey-Overbeek) theory. The DLVO theory considers the diffuse layer interactions between like-charged platelets to be entirely repulsive at all separations, and any attraction is attributed to van der Waals forces. However this fails to accurately describe the interaction between platelets in almost all cases, except for conditions where there is a low presence of counterions and low surface charges (McBride and Baveye, 2002; Mitchell and Soga, 2005; Wu et al., 1998). Thus, for most applications, including for kaolinite platelets, the DLVO theory is not able to accurately predict platelet interactions and notably fails to explain the significant attraction observed between like-charged colloids in the presence of an electrolyte (McBride and Baveye, 2002).

Despite the above controversy, it remains accepted that net interaction curves for two interacting colloids are of the forms illustrated in Fig. 3. For this reason, in this work a general interaction law is used which can reproduce the force-separation curves depicted in Fig. 3. This enables qualitatively correct particle interactions to be modelled easily, which can be adjusted to implicitly account for varying chemistry, whilst also allowing direct calibration of particle interactions if the force-separation curves are known. In summary, this work presents DEM simulations which for the first time feature realistic and independent interactions between the edges and/or faces of platelets, and which are correctly implemented and repeatable.

### 2.2.2. DEM implementation

To capture the interaction regimes depicted in Fig. 3, a simple *sphere-to-sphere* interaction law relating the normal force  $F$  to separation  $r$  is implemented which has the form:

$$F = A[r^{-\alpha} - r^{-\beta}] + B(1 - L(r)) \tag{1}$$

where  $\alpha > \beta$ , the parameters  $A, B, \alpha, \beta$  are constants which define the shape of the interaction law.  $L$  is the logistic function:  $L(r) = 1 / (1 + e^{-k(r-r_0)})$ , which ensures  $F$  in Eq. (1) converges to zero at long-range, and may be shifted and scaled using  $r_0$  and  $k$  depending on the maximum range of interactions. If  $B$  is set to zero, Eq. (1) resembles the well-known Lennard-Jones equation (if  $\alpha = 12, \beta = 6$ ), and

provides no long-range repulsion (red curve in Fig. 3). The parameters  $A$  and  $B$  control the local minimum (attractive) and local maximum (repulsive) peak forces, as well as the closest location at which the net force is zero (equilibrium position). The exponents  $\alpha$ ,  $\beta$  mainly determine the curvature and close-range stiffness.

Eq. (1) is applied between all sphere-to-sphere interactions, which means that for two of the platelets depicted in Fig. 1, several thousand individual interactions exist when aligned face-to-face. However, different parameters are used depending on the pair of interacting spheres (e.g. two face spheres will use a different interaction law compared to between an edge sphere and a face sphere). The interaction between two spheres (the force-separation curve) is unique, and depends only on Eq. (1). The platelet-to-platelet interactions in contrast depends on the parameters used in Eq. (1) as well as the type and number of individual sphere-to-sphere interactions (which depends on the platelets' relative positions and orientations). A key feature of this simple interaction law compared to previous work is that it provides an entirely smooth force-separation curve, and does not allow/include physical overlap between spheres. No separate tangential interaction law is implemented between any spheres, all interactions between spheres are normal and use Eq. (1). This means that the tangential behaviour between platelets is primarily governed by the platelet geometry. The platelets used in this study demonstrate a coefficient of friction of 0.03–0.05 when sheared, which was considered reasonable for molecularly smooth, adhesive surfaces (Gao et al., 2004). It should be noted that in previous studies modelling platelets using spheres, the regular lattice-spacing of the spheres would result in anomalous behaviour when the lattices are aligned and the platelets interlocked.

A total of 5 different classes of interactions (or ‘contacts’) may exist: *face-to-face* (FF), *edge-to-face* (EF), and *edge-to-edge* (EE) between platelets, and *face-to-wall* (FW) and *edge-to-wall* (EW) between platelets and boundaries. Although the platelets never ‘touch’, two platelets are considered ‘in contact’ when they are in close proximity with an interaction force acting between them.

For simplicity, in this exploratory work interactions with the sample boundaries (rigid walls) are treated as interactions with

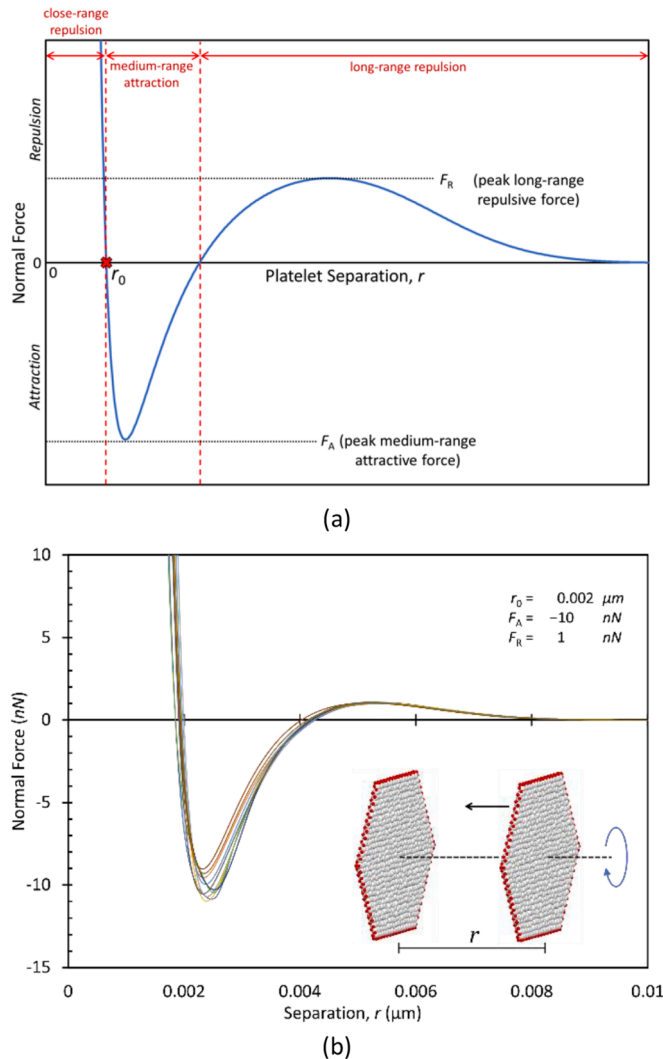


Fig. 4. Generalised force-separation plot (a); example force-separation plot for 2 face-to-face platelets (b).

particle faces. That is, edge-to-wall and face-to-wall interactions are calibrated to exhibit the same behaviour as edge-to-face and face-to-face platelet interactions, respectively. Thus, for each simulation shown, only 3 different interactions are described: *face-to-face*, *edge-to-face*, and *edge-to-edge*. For each of these 3 types of interaction, the parameters in Eq. (1) are calibrated to produce the desired macroscopic interaction, using the procedure outlined in de Bono and McDowell (2022). This is achieved by measuring the overall force between two platelets as a function of separation numerous times with random orientations, and adjusting the parameters accordingly. Any desired *platelet* interaction is specified in terms of  $r_0$ ,  $F_A$ ,  $F_R$ , as illustrated in Fig. 4(a). To achieve this net interaction, using given values of  $\alpha$  and  $\beta$ , the parameters  $A$  and  $B$  in Eq. (1) are adjusted until the net normal force (or stress) as a function of separation, measured from repeatedly driving two platelets towards each other with different orientations is correct. An example force-separation plot is shown in Fig. 4(b) for face-to-face interaction, which shows the repeatability (without the random internal translations of the platelet spheres, such a response would not be possible—if the spheres were hexagonally aligned, the force-separation curve would not be repeatable nor smoothly defined).

### 3. DEM simulations

#### 3.1. Simulation procedure

The simulations are performed using the software PFC3D (Itasca, 2015). All of the clay samples used here are created by generating several thousand platelets and then allowing them to settle under gravity. The initial cylindrical container is 10  $\mu\text{m}$  in diameter and 20  $\mu\text{m}$  in height. An arbitrary solid fraction of 0.06 was chosen, which results in 3628 platelets, all of which have the same diameter and thickness (1 and 0.04  $\mu\text{m}$ , respectively). The platelets used are the same as those shown in Fig. 1, giving approximately 3,000,000 spheres in total in each simulation. This is clearly a small number of platelets for a sample of clay, however it represents an improvement in terms of the number of particles and/or aspect ratios used in the related previous particle-based numerical studies. The samples are unlikely to constitute true representative element volumes, comparisons are primarily only made between simulations prepared and executed identically; no quantitative calibration is attempted with real experimental data, which mitigates such concerns at this stage (although qualitative comparisons will be made); the focus here is to elucidate the possible ‘mechanics’ of compression of clay based on hypothesised platelet interactions; calibration against alternative real clay data will be the subject of future research.

The platelets are created at random positions and are then allowed to settle, which is judged to have completed once the velocities have approached zero. To facilitate the gradual dissipation of kinetic energy from the system during settling, the velocities of all platelets are periodically and proportionally reduced by a small factor (1% every 0.0001 s), which broadly mimics the effects of viscous drag. This crude approach is similar in principal to that used by Sjoblom (2015) (although without additionally simulating random thermal perturbations), and is necessary to achieve a steady state. (A steady state could be achieved by implementing viscous damping at contacts.)

Following settlement, the samples are then subjected to one-dimensional compression tests. These are performed by applying increasing increments of load to the top boundary of the sample, by using a servo control which applies a vertical displacement to the top boundary until the desired load is met. In these simulations, a very low damping coefficient (0.02) is used to reach equilibrium.

#### 3.2. Characteristic platelet interactions

To evaluate the suitability of both the interaction law and the method of modelling the platelets two different platelet interaction regimes were initially simulated. The aim was to replicate well-documented characteristic particle interactions, capture the salient features of each and provide a basis for further DEM simulations. The choice of interaction regimes initially studied is analogous to key experimental comparisons made by others; qualitative comparisons are made where appropriate.

The two initial particle interaction regimes simulated use combinations of the particle interactions shown in Fig. 3, and are shown schematically in Fig. 5. Across the both regimes, all classes of interactions have stiff close-range repulsion, and medium-range attraction. The key difference is in the long-range repulsion for EF interactions.

In the first simulation (*Simulation A*), all 3 types of particle interactions (FF, EF, EE) are repulsive at long-range, with an attractive region at medium separation. This regime may be considered as representing neutral-to-slightly alkaline conditions where kaolinite

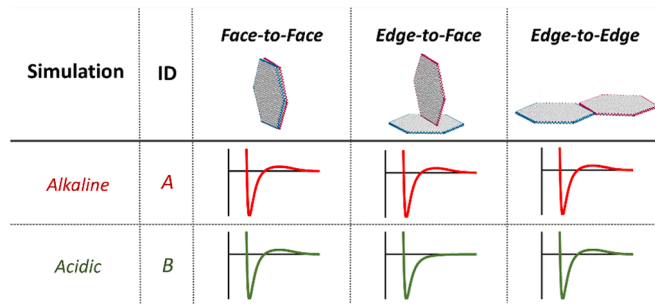


Fig. 5. Visual summary of the interaction regimes in simulations A & B

particles are assumed to have negative surface charges on both edges and faces, and with minimal electrolyte content. All three types (FF, EF, EE) of particle interactions have the same shaped force-separation curve, but the magnitudes of forces are smaller for EF and EE interactions due to the smaller ‘contact area’ (detailed below). For all interactions (FF, EF, EE), the long-range peak repulsive force was provisionally set at one tenth of the peak attractive force ( $F_R = -F_A/10$ ).

The second simulation (B) is identical except that there is no long-range repulsion for edge-to-face (EF) interactions, which are therefore predominantly attractive. This simulation seeks to replicate mildly acidic conditions in which the platelet edges possess positive surface charges (e.g Pedrotti and Tarantino, 2017.; van Olphen, 1963).

The magnitude of attraction and repulsion for the various platelet interactions can be characterised by the values  $F_A$  and  $F_R$ , as illustrated in Fig. 4(a). In all simulations,  $r_0$  was set at  $0.002 \mu\text{m}$ , and  $\alpha, \beta$  were set as 6, 5, respectively. The parameters  $k, r_0$  in the logistic function were set at 1000, 0.004, respectively. The maximum extent of all platelet interactions was set at  $0.010 \mu\text{m}$ —platelets separated by a distance greater than this are assumed to have no interactions (and are not ‘in contact’). To run full simulations with this number of spheres/platelets, it is necessary to set such a maximum interaction range that avoids an excessive number of interactions. Ideally, interactions at all separations would be computed, regardless of how far and how small the interaction forces are, however computing an extremely large number of sphere-to-sphere interactions each timestep would make dense states at high stresses unachievable. The (arbitrary) value of  $0.010 \mu\text{m}$  is the same as used by Sjoblom (2015), and very similar to the maximum interaction ranges used by others modelling kaolinite (Jaradat and Abdelaziz, 2019; Yao and Anandarajah, 2003). It is also broadly consistent with the range of interaction observed from atomic force microscopy experiments on kaolinite particles (e.g Gupta and Miller, 2010.).

For face-to-face (FF) interactions, in all three simulations the peak attractive force  $F_A$  was chosen arbitrarily and provisionally to be  $F_A = 10 \text{ nN}$  (equivalent to  $\approx 15 \text{ nN}/\mu\text{m}^2$ ). The peak attractive force for all EF and EE interactions was set at one twentieth (1/20) of this due to the smaller contact area (equivalent to  $\approx 25 \text{ nN}/\mu\text{m}^2$ ). For interactions with long-range repulsion, the peak repulsive force  $F_R$  was set at one tenth (1/10) of the peak attractive force. The individual effects of the magnitudes of the peak repulsive and attractive forces will be investigated in subsequent simulations. Details of the platelet interactions used in these and subsequent simulations are summarised in Table 1.

### 3.3. Sedimentation

Allowing the 2 samples to settle under gravity immediately demonstrates the effects of the particle interactions. The alkaline simulation (A) settles to a voids ratio of around 3, whilst the acidic simulation (B) forms a voluminous structure which extends throughout the enclosing cylinder, giving the maximum possible voids ratio of around 15 Fig. 6. shows a comparison of simulations A and B (alkaline versus acidic) following settlement.

The alkaline simulation (A)—with predominant repulsion at long range—settles to a denser, more compact sediment, which correctly reflects laboratory observations: for example Wang and Siu (2006a) and Pedrotti and Tarantino (2017) both prepared kaolin samples and measured sediment voids ratios of around 3–4 and 8–9 for alkaline and acidic fluids, respectively (see also Melton and Rand, 1977b). The long-range repulsion experienced by all particle interactions in this alkaline simulation allow the platelets to easily slide past one another before coming to rest horizontally due to gravity. The sample in simulation B forms a sediment with a larger volume than A; the platelets readily associate edge-to-face, forming a voluminous three-dimensional structure. A separate simulation (not shown), in which all interactions were predominantly attractive (not just EF) produced very similar behaviour to simulation B. This suggests that EF interactions (or collisions) determine the loosest possible structure, at least for the solid fraction and sample size considered here (see Melton and Rand, 1977b, who suppressed all particle repulsions by increasing the electrolyte content in an alkaline fluid).

Although the sedimentation demonstrated by the two samples here is broadly consistent with experimental observations (e.g Pedrotti and Tarantino, 2017.), it must be emphasised that the purpose was not to precisely capture or study the settling, which is itself a complex process and would require explicit consideration of the fluid and drag forces etc. (the aim was instead to create initial samples ready for compression tests). The fact that the samples produce the qualitatively correct sediments one would expect from the particle interactions is reassuring and supports the approach used here to model particle interactions. It should be noted that the simulations are highly idealised: they all have a uniform platelet size and no Brownian motion is simulated during settlement—which would likely cause some particles to overcome long-range repulsive barriers and flocculate.

**Table 1**  
Summary of interaction regimes in simulations.

ID	Name	Face-to-Face		Edge-to-Face		Edge-to-Edge		Notes
		$F_A$	$F_R$	$F_A$	$F_R$	$F_A$	$F_R$	
A	‘alkaline’	-10	1	-0.50	0.05	-0.50	0.05	All interactions predominantly repulsive at long-range
B	‘acidic’	-10	1	-0.50	0	-0.50	0.05	As A, but with predominantly attractive EF interactions
C	‘acidic’	-1	0.1	-0.05	0	-0.05	0.005	As B, but interactions scaled by 0.1
D	‘acidic’	-100	10	-5	0	-5	0.5	As B, but interactions scaled by 10
E	‘increased attraction’	-200	10	-10	0	-10	0.5	As D, but magnitude of medium-range attraction scaled by 2
F	‘increased repulsion’	-100	50	-5	0	-5	2.5	As D, but magnitude of long-range repulsion scaled by 5

Values of  $F_A, F_R$  are given in units of nN. The values given refer to idealised interactions with maximum contact area.

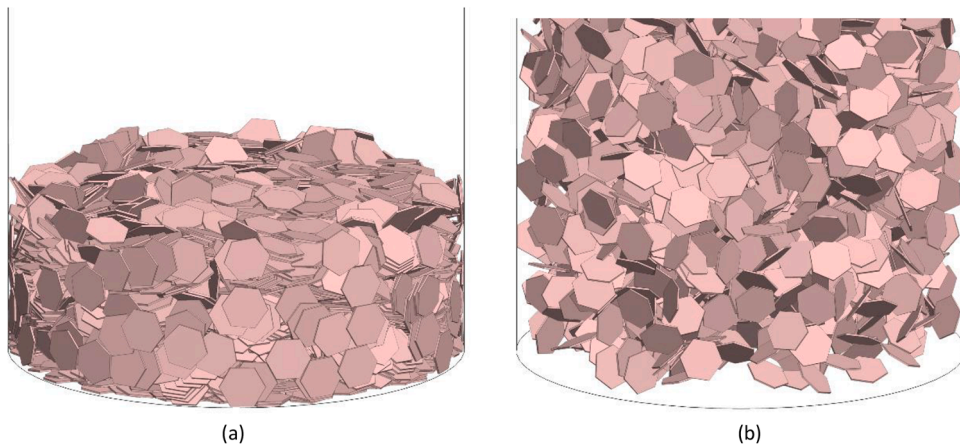


**Fig. 6.** Images of samples following settlement: Alkaline (a); and Acidic (b). The alkaline simulation features predominantly repulsive interactions, the acidic simulation includes predominantly attractive edge-face interactions.

3.4. One-dimensional compression

The one-dimensional compression results for the two simulations in terms of voids ratio and log stress ( $e, \sigma$ ) are given in Fig. 7(a). Despite initially having a far higher voids ratio, simulation B readily compresses, and the two responses appear to merge at stresses above 10 kPa. Initially, under no load, the sample in simulation B consists of a voluminous, EF flocculated structure, as stress is applied the structure gives way, the platelets reorientate themselves and more FF platelet contacts are formed. Both sample appear physically similar at the end of the tests, shown in Fig. 7(a) is the acidic sample at an applied load of 12.8 kPa. A qualitative comparison can be made with the experimental results shown in Fig. 7(b), reproduced from Pedrotti and Tarantino (2017) (see also Wang and Siu, 2006b) Fig. 7.(b) shows analogous one-dimensional compression results comparing kaolin samples prepared with acidic (pH 4) and alkaline (pH 9) fluids. The same trend can be seen where the acidic sample initially exhibits a higher voids ratio, and upon loading appears to compress more rapidly. The alkaline sample in comparison, in which all types of interactions have long-range repulsion, is initially denser.

Each simulation typically contains several million sphere-to-sphere interactions. These can be filtered and reduced to several thousand platelet-to-platelet ‘contacts’ (platelets in close proximity which are interacting). These platelet-to-platelet contacts can then be further subdivided into face-to-face, edge-to-face and edge-to-edge interactions. The criteria for identifying the type of interaction for each contact is based on the following ordered set of rules: given  $X$  number of interactions between two platelets, if all of these are between edge spheres, then the contact is classed as edge-to-edge. If  $X$  consists of interactions between only edge spheres in one

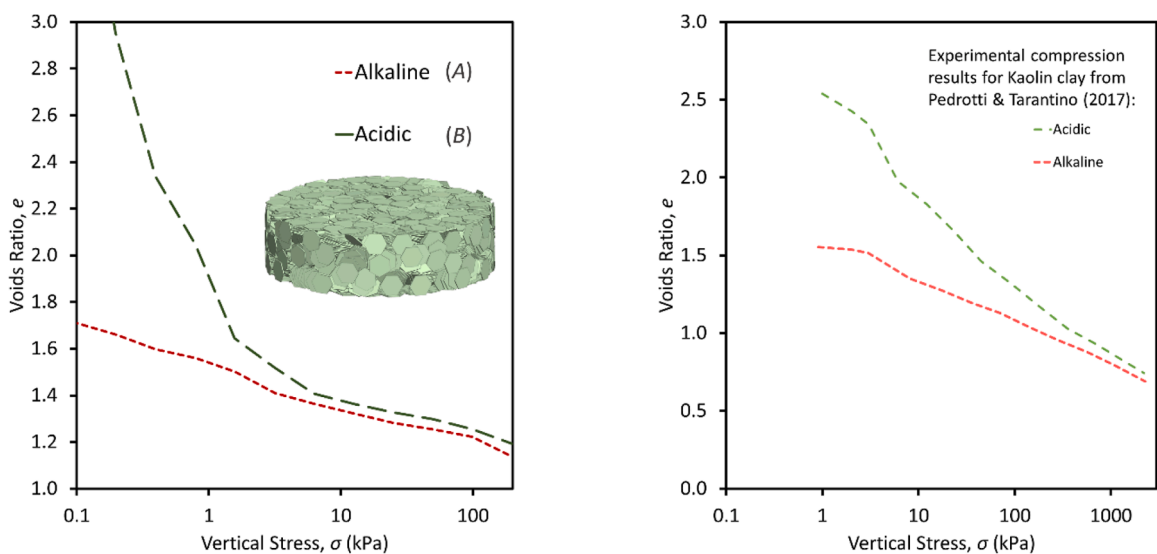


**Fig. 7.** One-dimensional compression results for the 2 simulations (a), and comparable experimental results for compression of kaolin clay from Pedrotti and Tarantino (2017) (b); comparing behaviour of acidic and alkaline samples.



platelet, then the contact is classed as edge-to-face. If  $X$  consists of interactions between exclusively facial spheres, then it is classed as face-to-face. If  $X$  consists of interactions between a combination of edge spheres and facial spheres, then the relative orientation is used: if the platelets are parallel ( $+/- 2^\circ$ ) then the contact is classed as face-to-face; if the platelets are not parallel it is classed as edge-to-face. Although this division between EF/FF contacts is arbitrary, it was confirmed via visual inspection of the DEM samples. Adjusting this criterion (i.e. using a greater cut-off angle) does not materially change the data, and the same overall trends are observed.

Fig. 8 shows the evolution of different types of platelet-to-platelet contacts throughout the alkaline and acidic simulations. In both simulations, the total number of contacts increases as the materials compress. In the alkaline simulation (A), at the initial state there are a significant number of all types (FF, EF, EE). This simulation begins from a state in which the platelets are largely aligned in the horizontal direction. As stress increases there is a slight reduction in the number of EE contacts, while the number of FF contacts remains fairly steady before increasing slightly at large stresses. There is an overall increase in EF contacts as the sample compresses, which accounts for most of the overall increase in contacts. In the acidic simulation, the initial sample has fewer overall contacts due to the looser state, and there is an increase in all types (FF, EF, EE) during the test. Like the alkaline test, the number of EF contacts increase the most significantly, however in contrast FF contacts form later at higher stresses. The final states across both simulations display similar contact distributions.

### 3.5. Effects of the interaction laws

#### 3.5.1. Magnitude of particle interactions

From these initial simulations as well as earlier exploratory work (not shown), it emerged that multiplying the platelet interaction curves (i.e. multiplying  $F_A$  and  $F_R$ ) by a scalar changes the location of the compression curve. Using the acidic simulation (B) as the benchmark, Fig. 9 shows the results from two further acidic simulations (C, D in Table 1), in which the platelet interactions (forces  $F_A$  and  $F_R$ ) have been multiplied by factors of 0.1 and 10, respectively. The normal compression curves are shifted along the stress axis by the same factor by which their interaction laws are scaled (hence equidistant on the log stress scale). An additional general observation from the simulations is also noted in Fig. 9, which is that the compressibility at high stresses and low voids ratios (as well as any unloading response) is directly influenced by the close-range stiffness between platelets.

#### 3.5.2. Effects of attractive and repulsive forces

A further set of simulations is now presented which aims to show the separate effects of the magnitudes of attractive and repulsive forces used in the interaction law, with a view to evaluating the suitability and implications of such input parameters; and ultimately to determine the role of the particle interactions with regard to the compressibility.

The acidic simulation D (with scaled up peak interaction forces) is compared with two further simulations: one with increased attraction and one with increased repulsion (E, F in Table 1). Note that there is still no long-range repulsion for edge-to-face interactions. This set of platelet interaction regimes is illustrated in Fig. 10(a), and the compression results are given in Fig. 10(b). The compression line for the simulation with increased attraction is again shifted to higher stresses, showing that the degree of attraction between platelets (specifically EF interactions) is the most dominant factor in determining the location of the compression line and any apparent virgin yield strength of the material. The simulation with increased repulsion (for face-to-face and edge-to-edge interactions) initially appears to coincide with the benchmark case, however at higher stresses it appears that the increased long-range repulsion resists face-to-face aggregation of the platelets, resulting in very-slightly higher voids ratios.

Fig. 11(a)–(c) show the changing numbers of face-to-face, edge-to-face and edge-to-edge contacts throughout the three simulations.

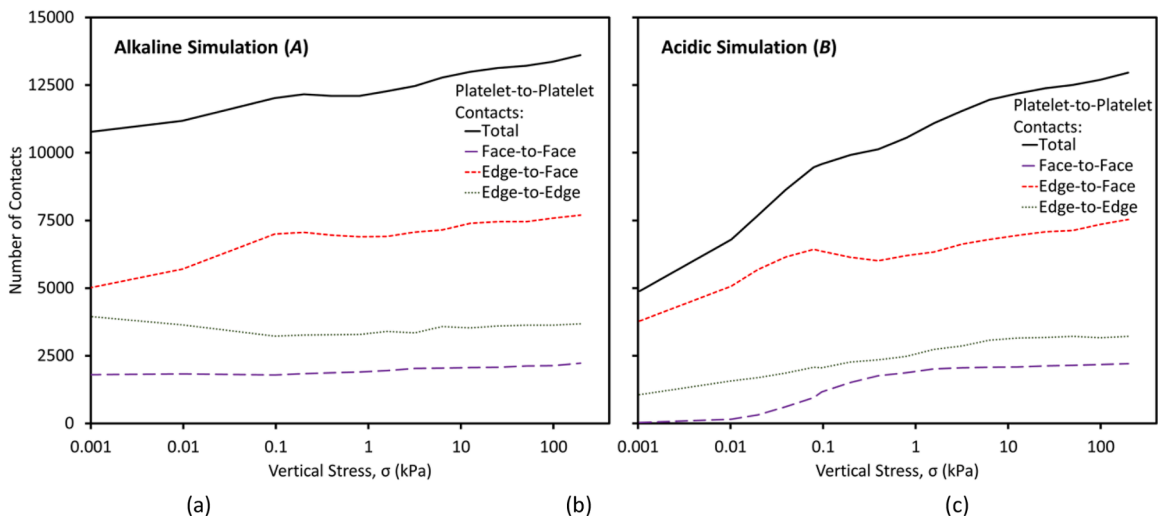


Fig. 8. Figures showing evolution of different types of contacts (interactions) in alkaline (a), acidic (b) and high salt content (c) simulations.

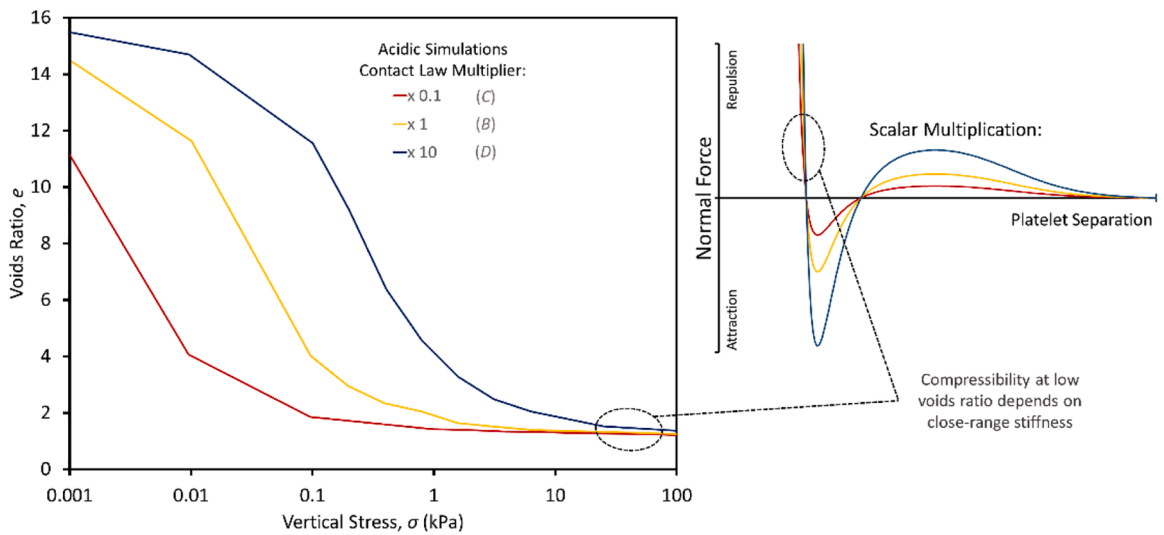
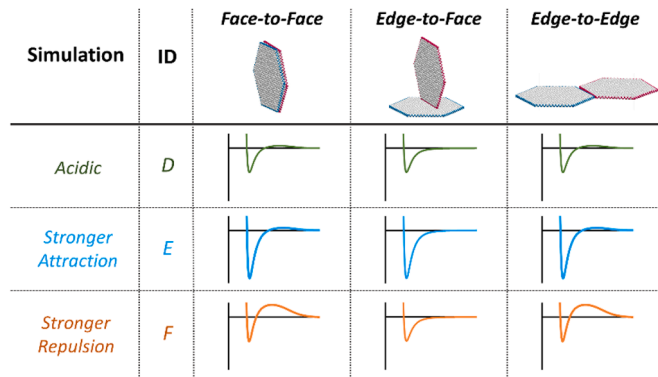
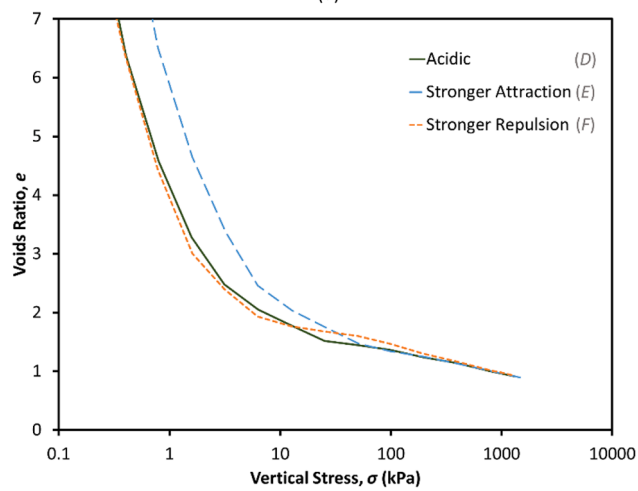


Fig. 9. Effects of scaling particle interactions for the acidic clay and effect of close-range stiffness.



(a)

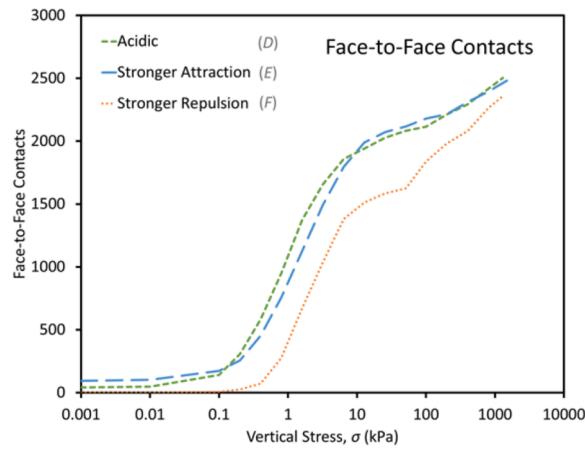


(b)

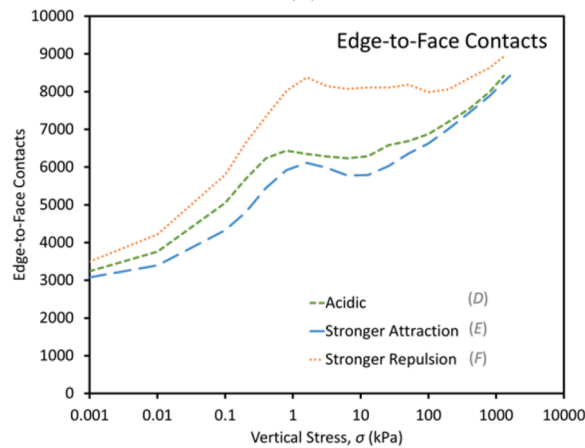
Fig. 10. Summary of interaction regimes used (a); and one-dimensional compression results for simulations with varying attractive and repulsive interactive forces (b).

The benchmark acidic simulation (*D*), and the simulation with stronger attraction (*E*) display largely identical behaviour with a small offset between the curves. The simulation with stronger repulsion (*F*) exhibits distinct behaviour, with a much greater number of EF contacts, and a delayed increase in the number of FF contacts. At the highest stresses reached, the simulations appear to be converging to the same contact distribution.

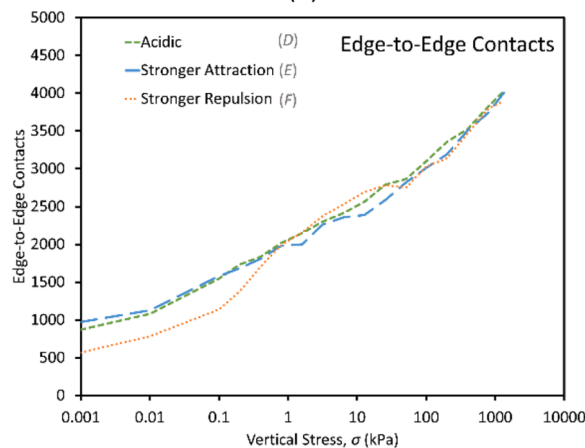
For any sample, as one would anticipate, there is a general increase in all types of contacts as the sample decreases in volume. What



(a)



(b)



(c)

**Fig. 11.** Variation in numbers of contacts during compression tests: Face-to-Face contacts (a); Edge-to-Face contacts (b); Edge-to-Edge contacts (c). Note the different scales on the y-axes.

the plots in Fig. 11 appear to reveal is that there is a marked transition or ‘biting point’ (we might be tempted to call this virgin ‘yield’) at which stage the rapid increase in EF contacts is temporarily arrested, which coincides with the maximum rate of increase in FF contacts. This clearly indicates the onset of face-to-face aggregation, and the conversion of contacts from EF to FF. Comparing the benchmark acidic simulation (D) with the stronger attraction (E) simulation, shows that this transition occurs later, and corresponds to the shifted location of the compression line. This can be attributed to the stronger attraction between interacting EF platelets, which must be pulled apart in order for the platelets to aggregate face-to-face. Thus the simulations suggest that the attraction between particles, particularly between EF contacts plays a governing role in the virgin compressibility and yielding of the sample.

A similar trend/transition point is shown by the simulation with increased long-range repulsion (F), which has the same attraction holding EF platelets together as in the benchmark case (D). However in this case (F) the increased FF repulsion makes it harder for platelets to aggregate face-to-face. The stronger FF repulsion in particular appears to contribute to more EF contacts—which would be the preferred position for two approaching (repulsive) facing platelets. This ultimately means more confinement is required to force platelets to overcome the long-range repulsion and aggregate face-to-face.

### 3.6. Contact analysis and platelet aggregation

A final analysis is now presented, which explores the behaviour of platelet-to-platelet contacts during unloading and looks in more

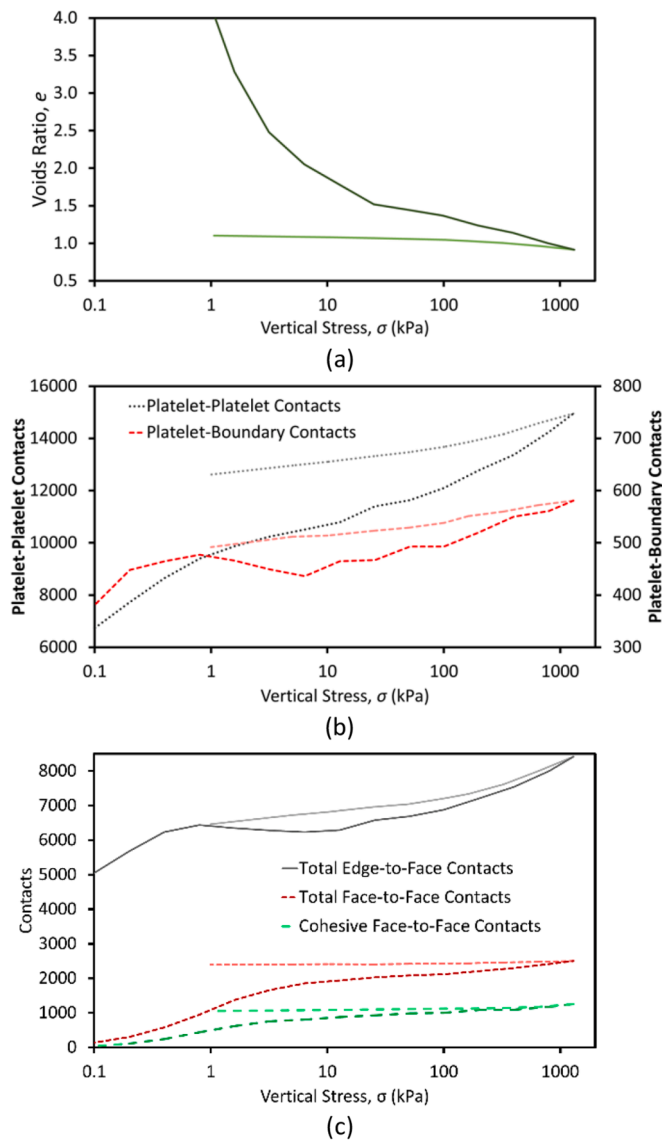


Fig. 12. Acidic simulation unloading response from high stress (a); overall number of contacts during loading and unloading (b); edge-to-face and face-to-face contacts during loading and unloading (c).

detail at the formation of platelet stacks (aggregation). Fig. 12(a) shows the unloading response from the highest stress reached (1280 kPa) in the acidic simulation (D). As one would expect, the unloading response is much stiffer than the virgin loading, with minimal change in volume, and appears stiffer than any unloading lines obtained in previous particle-based studies. This stiff unloading response, consistent with real clays (e.g. Chen et al., 2000.), reinforces the suitability of the interaction laws, and also the importance of the close-range particle stiffness. If linear spring interaction laws were used for example, and/or a lower stiffness, there would be less permanent volume change during compression, and the unloading response would be more elastic. Fig. 12(a) reveals that a significant amount of irreversible deformation has occurred during compression. This is also evident from the residual increase in the number of contacts (interaction platelets) after unloading: Fig. 12(b) shows the total numbers of platelet-to-platelet and platelet-to-boundary contacts. The contacts between platelets and boundaries only make up a small proportion of the overall contacts, of which most are with platelet edges. These overall measures of contacts both decrease upon unloading. This decrease upon unloading is mainly contributed to by a loss of edge-to-face contacts; in contrast, the number of face-to-face contacts displays a negligible decrease during unloading from 1280 to 1 kPa, shown in Fig. 12(c).

Also shown in Fig. 12(c) is the number of ‘cohesive’ face-to-face contacts. Cohesive contacts refer to interacting parallel platelets where the long-range repulsion has been overcome and the platelets are comfortably held together, forming part of a ‘stack’ of at least 2 platelets. Cohesive contacts are identified in this instance simply as those face-to-face interactions in which the separation is less than or equal to  $r_0$  (0.002  $\mu\text{m}$ ). This location ( $r_0$ ) is the ‘default’ separation for two platelets once any long-range repulsion has been overcome—any further relative movement closer is quickly resisted by stiff repulsion, and relative movement away is opposed by the medium-range attraction. This separation (between two parallel FF platelets) is measured as the shortest distance from the centre of mass of one platelet to the central plane of the other, less the platelet thickness. The number of cohesive FF contacts increases approximately linearly with the overall number of face-to-face contacts and remains essentially unchanged upon unloading.

Fig. 13 provides histograms showing the frequencies of face-to-face separations from the acidic simulation, at the highest stress (a) and after unloading (b). At a vertical stress of 1280 kPa the most common separation between two face-to-face platelets is around 0.0015  $\mu\text{m}$ , reflecting the large compressive forces transmitted between particles (cf. Fig. 4(b)). However despite the very large inter-particle forces, the platelets are never in physical contact (overlapping), this is due both to the stiff close-range repulsion and the structure of the platelets which prevent any interlocking between spheres. Upon unloading, one can see that there is a relaxation and all such contacts revert back to a separation of around 0.002  $\mu\text{m}$  (the value of  $r_0$ ), where the net force is zero; these platelets remain aggregated (or ‘stacked’).

Fig. 14(a) displays the overall number of platelet stacks, formed by cohesive FF contacts, and the number of free individual platelets. Also plotted is the sum of these two quantities (termed ‘bodies’), representing the effective number of ‘mechanical’ particles. It is interesting to observe that the number of free platelets decreases more rapidly than the number of stacks increases; this reflects the formation of larger stacks which contain increasing numbers of platelets; i.e. the emergence of a distribution of stack sizes. As may be

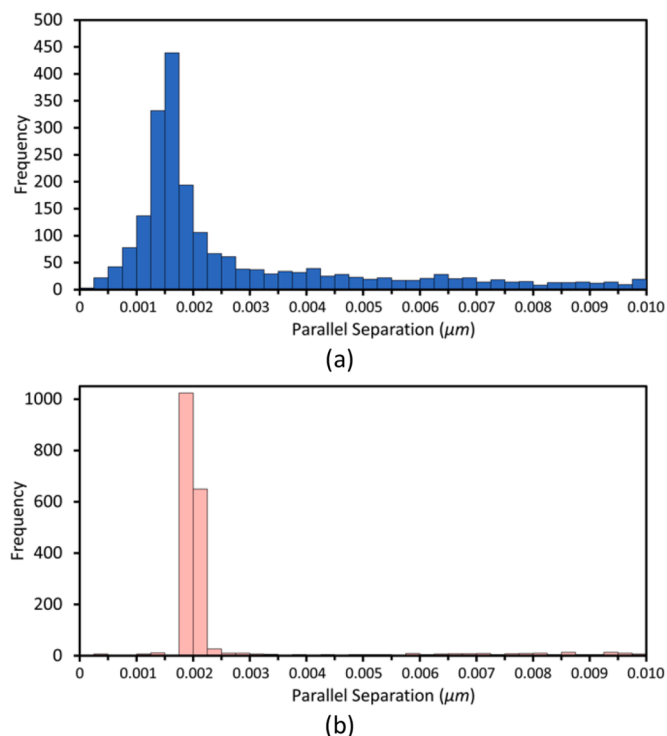


Fig. 13. Histogram showing separation between face-to-face platelets in acidic simulation (D) at 1280 kPa.

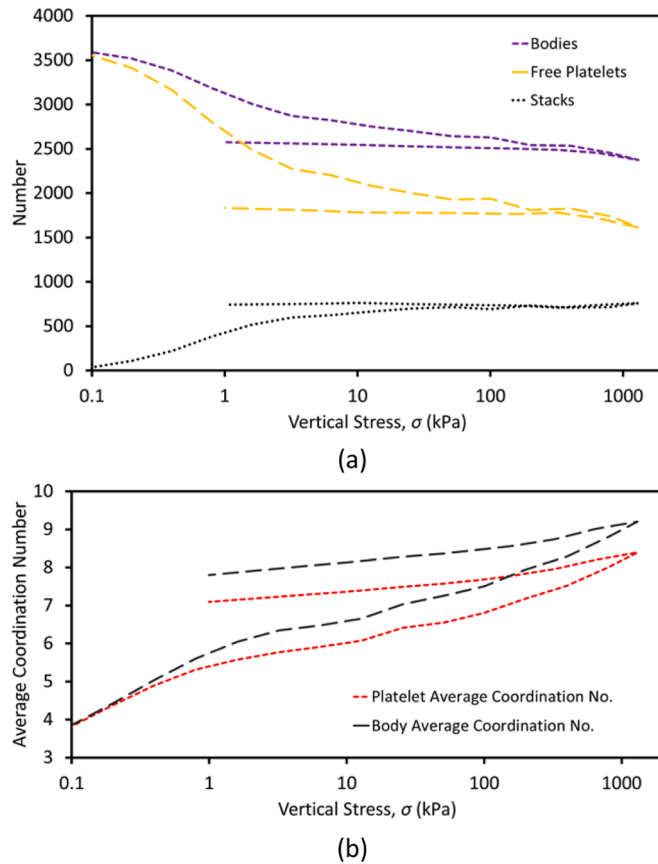


Fig. 14. Evolution of number of free platelets, stacks, and overall number of bodies (a); and average coordination number with respect to individual platelets and bodies (b).

inferred from the previous plots, this figure confirms that the number of aggregated stacks remains constant during unloading.

Shown in Fig. 14(b) is the average coordination number as a function of applied stress. This is plotted in the standard way, i.e. the average number of ‘contacts’ per platelet, and also in terms of ‘bodies’ (including both free and aggregated groups of platelets). This latter method treats each stack as a single object and does not consider the interactions/contacts between platelets in any stack. The average coordination number per platelet simply reflects the overall number of contacts, as there are a fixed number of (unbreakable) platelets, however the ‘body’ coordination number is a function of both the contacts and number of stacks, and displays a more rapid increase during compression.

Fig. 15 shows a cross-section of the sample at the ultimate stress of 1280 kPa, with individual platelet stacks highlighted using different colours. In spite of the uniform platelet size and shape, the general fabric displayed by the platelets is consistent with that revealed in images of real samples after compression, e.g. Delage and Lefebvre (1984).; see also images in Mitchell and Soga (2005), Wang and Siu (2006a), Pedrotti and Tarantino (2017). Although the platelets are generally aligned in the horizontal plane, the platelets still display noticeable random orientations, there are also obvious voids visible. Also highlighted in Fig. 15 is an example of a large stack of 8 platelets. This stack effectively acts as a single entity, and although scarcely visible in the figure, the platelets are not physically touching. This is due to both the stiff close-range repulsion, and due to the structure of the platelets (recall we have eliminated the regular array nature of the spheres in the platelet plane) which prevent any interlocking between spheres.

Fig. 16 shows the stack size distributions obtained from all major simulations discussed here, with stack size measured simply as the number of platelets in a stack. As one might expect, single platelets are the most common, followed by stacks consisting of two platelets, with larger stacks decreasing in frequency Turcotte (1986). states that if the number  $N$  (of objects) with a characteristic linear dimension greater than  $L$ , is given by  $N \sim L^{-D}$ , then a fractal is defined with  $D$  as the fractal dimension. Given the prevalence of fractal size distributions in crushable granular soils, and the known relationship that fractal size distributions have to space-filling (Anishchik and Medvedev, 1995; de Bono and McDowell, 2020), it follows that a fractal distribution may well emerge from the aggregation of platelets during the compression (and densification) of clay. Taking the number of platelets in a stack (or the stack height) as the characteristic linear dimension, then it does tentatively appear in Fig. 16 that the stack distributions are approaching a fractal with a dimension of 2.5.

It has been shown and accepted that sands and clays display the same basic behaviour under compression, and that the irreversible volume change for sands is due to the evolution of a fractal size distribution due to crushing McDowell et al. (1996). for example have

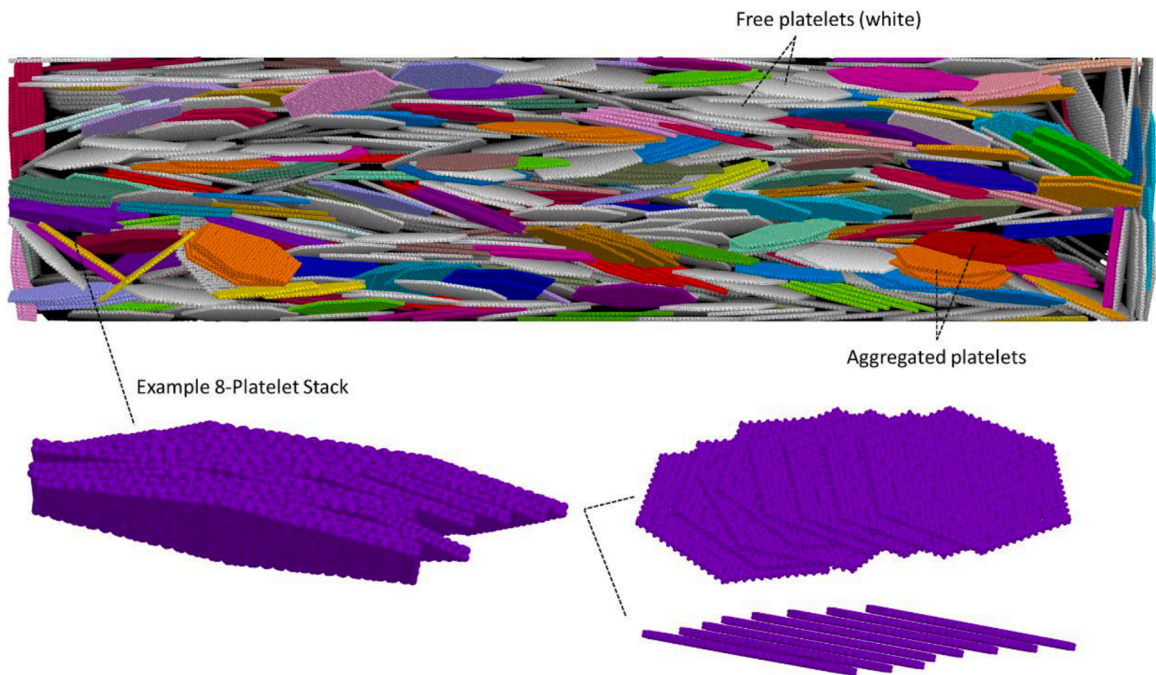


Fig. 15. Cross section of acidic sample at ultimate stress, showing coloured stacks of aggregated platelets.

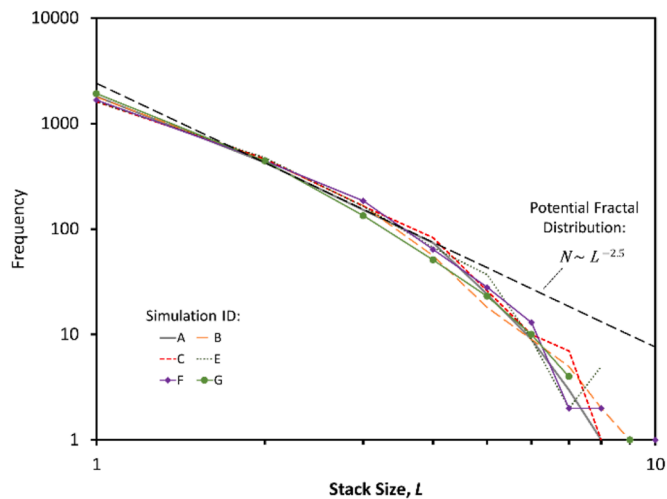


Fig. 16. Graph showing stack size distributions from all major simulations.

examined the fractal nature of soils in which a distribution of particle sizes emerge during normal compression. It has long been questioned whether a similar type of mechanism is responsible for the space filling of the voids as a clay compresses. The evidence from these simulations support this view; this is, to the authors’ knowledge, the first time that there is any evidence to support a similar phenomenon existing for clay to that of sand, whereby a fractal distribution of macro-particles (‘stacks’ or ‘peds’) emerges during normal compression De Bono and McDowell (2020). showed that the emergence of a fractal with a dimension of 2.5 could be explained by the tendency of a soil to try to achieve an Apollonian packing, with a voids ratio tending towards zero, as the distribution of sizes becomes wider such as to be able to fill the space available. This paper would therefore support the notion that virgin compression is in fact the phenomenon of ‘space-filling’ via the production of a distribution of macro-particle sizes or stacks.

Sands and clays also display the same basic behaviour under shearing; indeed, clays are usually found to have a critical state angle of friction at large shear strains. In the simulations presented here, no friction is directly implemented between the platelets. However, it is possible to gain some insight to the frictional strength of the material by considering the horizontal stresses that arise in the clay during normal compression. The ratio of horizontal to vertical stress ( $K_0$ ) in soils is known to follow  $K_0 = 1 - \sin\phi$  (Jaky, 1948) during

virgin compression. The simulations here consistently give  $K_0 = 0.85$ , implying a (e.g. critical state) friction angle of  $\approx 9^\circ$ , or alternatively from Mohr's circle a mobilised friction angle in one-dimensional compression of  $5^\circ$ . Given that no particle friction is explicitly included in this model, this apparent bulk friction must be a function of particle shape (or more precisely the stack shapes), and presumably also the strength of attractive forces. Further simulations are clearly needed to fully understand what particle-scale mechanisms occur during shearing, and how these govern the bulk frictional strength, in addition to establishing the effect of including an interparticle coefficient of friction directly; however, this is beyond the scope of this paper. It should also be possible to clarify the role of friction on the plastic compressibility of the soil, given the evidence of a possible relationship between friction angle and plasticity index (Wood, 1990).

#### 4. Concluding remarks

The aim of this work was to demonstrate an effective method of simulating clay realistically and correctly using the discrete element method, and to provide a basis for further, more advanced studies which will ultimately lead to new understandings on what governs the macroscopic behaviour of clay.

A fresh attempt to simulate clay using DEM was shown, which uses a new and straightforward interaction law that can reproduce well-known characteristic platelet interactions. Kaolinite platelets were modelled with a realistic size and shape, notably with a high aspect ratio of 25. A brief sensitivity analysis of the interaction law was performed which demonstrated the general effects of varying the magnitude of attractive and repulsive forces acting between the platelets. By adjusting the input parameters for the interaction law, to implicitly reflect a range of variables such as the pH and/or electrolyte content, the model was able to capture the qualitatively correct sedimentation and compression behaviour that one would expect.

For the purpose of providing a basis for more advanced subsequent investigations, the simulations shown here were all simplified (e.g., uniform particle size distribution, no Brownian motion and limited variation of platelet interactions). However, despite their simplified nature, tentative analysis revealed useful insights into the roles of long-range attraction and repulsion, platelet aggregation, and the compressibility.

The paper has shown that virgin compression is largely dominated by the breakdown or 'fracture' of edge-to-face 'contacts'— and the formation of aggregated stacks, having a fractal distribution of sizes, such that the reduction in voids ratio under increasing stress, through the emergence of a distribution of stack sizes and space-filling, bears much resemblance to the virgin compression of sand and the emergence of a fractal size distribution by crushing.

#### CRediT authorship contribution statement

**John P. de Bono:** Conceptualization, Software, Investigation, Writing – original draft, Writing – review & editing. **Glenn R. McDowell:** Project administration, Funding acquisition, Resources, Writing – review & editing.

#### Declaration of Competing Interest

The authors declare that they have no known competing financial interests or personal relationships that could have appeared to influence the work reported in this paper.

#### Acknowledgments

This work was supported by the Engineering and Physical Sciences Research Council [grant number EP/S016228/1].

#### References

- Aminpour, P., Sjöblom, K.J., 2019. Multi-scale modelling of kaolinite triaxial behaviour. *Geotech. Lett.* 9, 178–185. <https://doi.org/10.1680/jgele.18.00194>.
- Anandarajah, A., 2000. Numerical simulation of one-dimensional behaviour of a kaolinite. *Geotechnique* 50, 509–519. <https://doi.org/10.1680/geot.2000.50.5.509>.
- Anishchik, S.V., Medvedev, N.N., 1995. Three-dimensional apollonian packing as a model for dense granular systems. *Phys. Rev. Lett.* 75, 4314–4317. <https://doi.org/10.1103/PhysRevLett.75.4314>.
- Bandera, S., O'Sullivan, C., Tangney, P., Angioletti-Uberti, S., 2021. Coarse-grained molecular dynamics simulations of clay compression. *Comput. Geotech.* 138, 104333 <https://doi.org/10.1016/j.compgeo.2021.104333>.
- Bayesteh, H., Hoseini, A., 2021. Effect of mechanical and electro-chemical contacts on the particle orientation of clay minerals during swelling and sedimentation: a DEM simulation. *Comput. Geotech.* 130, 103913 <https://doi.org/10.1016/j.compgeo.2020.103913>.
- Chen, J., Anandarajah, A., Inyang, H., 2000. Pore fluid properties and compressibility of kaolinite. *J. Geotech. Geoenviron. Eng.* 126, 798–807. [https://doi.org/10.1061/\(ASCE\)1090-0241\(2000\)126:9\(798\)](https://doi.org/10.1061/(ASCE)1090-0241(2000)126:9(798)).
- de Bono, J.P., McDowell, G.R., 2022. Some important aspects of modelling clay platelet interactions using DEM. *Powder Technol.* 398, 117056 <https://doi.org/10.1016/j.powtec.2021.117056>.
- de Bono, J.P., McDowell, G.R., 2020. On the packing and crushing of granular materials. *Int. J. Solids Struct.* 187, 133–140. <https://doi.org/10.1016/j.ijsolstr.2018.07.011>.
- Delage, P., Lefebvre, G., 1984. Study of the structure of a sensitive Champlain clay and of its evolution during consolidation. *Can. Geotech. J.* 21, 21–35. <https://doi.org/10.1139/t84-003>.
- Ebrahimi, D., Pellenq, R.J.M., Whittle, A.J., 2016. Mesoscale simulation of clay aggregate formation and mechanical properties. *Granul. Matter* 18, 49. <https://doi.org/10.1007/s10035-016-0655-8>.
- Ebrahimi, D., Whittle, A.J., Pellenq, R.J.M., 2014. Mesoscale properties of clay aggregates from potential of mean force representation of interactions between nanoplatelets. *J. Chem. Phys.* 140, 154309 <https://doi.org/10.1063/1.4870932>.



- Gao, J., Luedtke, W.D., Gourdon, D., Ruths, M., Israelachvili, J.N., Landman, U., 2004. Frictional forces and Amontons' law: from the molecular to the macroscopic scale. *J. Phys. Chem. B* 108, 3410–3425. <https://doi.org/10.1021/jp036362l>.
- Gupta, V., Miller, J.D., 2010. Surface force measurements at the basal planes of ordered kaolinite particles. *J. Colloid Interface Sci.* 344, 362–371. <https://doi.org/10.1016/j.jcis.2010.01.012>.
- Itasca, 2015. PFC3D.
- Jaky, J., 1948. Pressure in silos. In: *Proceedings of the 2nd International Conference on Soil Mechanics and Foundation Engineering*, 1, pp. 103–107.
- Jaradat, K.A., Abdelaziz, S.L., 2019. On the use of discrete element method for multi-scale assessment of clay behavior. *Comput. Geotech.* 112, 329–341. <https://doi.org/10.1016/j.compgeo.2019.05.001>.
- McBride, M.B., Baveye, P., 2002. Diffuse double-layer models, long-range forces, and ordering in clay colloids. *Soil Sci. Soc. Am. J.* 66, 1207. <https://doi.org/10.2136/sssaj2002.1207>.
- McDowell, G.R., Bolton, M.D., Robertson, D., 1996. The fractal crushing of granular materials. *J. Mech. Phys. Solids* 44, 2079–2101.
- Melton, I.E., Rand, B., 1977a. Particle interactions in aqueous kaolinite suspensions I. *J. Colloid Interface Sci.* 60, 331–336. [https://doi.org/10.1016/0021-9797\(77\)90292-2](https://doi.org/10.1016/0021-9797(77)90292-2).
- Melton, I.E., Rand, B., 1977b. Particle interactions in aqueous kaolinite suspensions. III. Sedimentation volumes. *J. Colloid Interface Sci.* 60, 331–336. [https://doi.org/10.1016/0021-9797\(77\)90292-2](https://doi.org/10.1016/0021-9797(77)90292-2).
- Mitchell, J.K., Soga, K., 2005. *Fundamentals of Soil Behavior*, 3rd ed. John Wiley and Sons, Hoboken, New Jersey.
- Pagano, A.G., Magnanimo, V., Weinhart, T., Tarantino, A., 2020. Exploring the micromechanics of non-active clays by way of virtual DEM experiments. *Géotechnique* 70, 303–316. <https://doi.org/10.1680/jgeot.18.P.060>.
- Pedrotti, M., Tarantino, A., 2017. An experimental investigation into the micromechanics of non-active clays. *Géotechnique* 1–18. <https://doi.org/10.1680/jgeot.16.P.245>.
- Sjoblom, K.J., 2015. Coarse-grained molecular dynamics approach to simulating clay behavior. *J. Geotech. Geoenviron. ASCE* 142, 1–6. [https://doi.org/10.1061/\(ASCE\)GT.1943-5606.0001394](https://doi.org/10.1061/(ASCE)GT.1943-5606.0001394).
- Thureson, A., Ullner, M., Åkesson, T., Labbez, C., Jönsson, B., 2013. Monte Carlo simulations of parallel charged platelets as an approach to Tactoid formation in clay. *Langmuir* 29, 9216–9223. <https://doi.org/10.1021/la401272u>.
- Turcotte, D.L., 1986. Fractals and fragmentation. *J. Geophys. Res.* 91, 1921. <https://doi.org/10.1029/JB091iB02p01921>.
- van Olphen, H., 1963. *An Introduction to Clay Colloid Chemistry*. John Wiley and Sons, New York.
- Wang, Y.H., Siu, W.K., 2006a. Structure characteristics and mechanical properties of kaolinite soils. I. Surface charges and structural characterizations. *Can. Geotech. J.* 43, 587–600. <https://doi.org/10.1139/t06-026>.
- Wang, Y.H., Siu, W.K., 2006b. Structure characteristics and mechanical properties of kaolinite soils. II. Effects of structure on mechanical properties. *Can. Geotech. J.* 43, 601–617. <https://doi.org/10.1139/t06-027>.
- Wood, D.M., 1990. *Soil Behaviour and Critical State Soil Mechanics*. Cambridge University Press.
- Wu, J., Bratko, D., Prausnitz, J.M., 1998. Interaction between like-charged colloidal spheres in electrolyte solutions. *Proc. Natl. Acad. Sci.* 95, 15169–15172. <https://doi.org/10.1073/pnas.95.26.15169>.
- Yao, M., Anandarajah, A., 2003. Three-dimensional discrete element method of analysis of clays. *ASCE J. Eng. Mech.* 129, 585–596.